Altered Temporal-Parietal Morphological Similarity Networks in Non-Small Cell Lung Cancer Patients Following Chemotherapy: An MRI Preliminary Study

Gong Chen (xiaochengong@126.com)
UESTC: University of Electronic Science and Technology of China https://orcid.org/0000-0002-6275-9093

Chuan Wu
Sichuan Cancer Hospital and Research Institute: Sichuan Cancer Hospital and Institute

Yuan Liu
UESTC: University of Electronic Science and Technology of China

Zengyi Fang
Sichuan Cancer Hospital and Research Institute: Sichuan Cancer Hospital and Institute

Liping Luo
Sichuan Cancer Hospital and Research Institute: Sichuan Cancer Hospital and Institute

Xin Lai
Sichuan Cancer Hospital and Research Institute: Sichuan Cancer Hospital and Institute

Weidong Wang
Sichuan Cancer Hospital and Research Institute: Sichuan Cancer Hospital and Institute

Li Dong
UESTC: University of Electronic Science and Technology of China

Research Article

Keywords: Non-small cell lung cancer, Platinum-based chemotherapy, Morphological similarity network, Graph theory, Chemobrain

Posted Date: February 28th, 2022

DOI: https://doi.org/10.21203/rs.3.rs-1352789/v1

Abstract

Non-small cell lung cancer (NSCLC) accounts for more than 85% of all lung cancer cases, and chemotherapy-related brain changes (known as “chemobrain”) in NSCLC patients were found in previous studies. However, the effects of platinum-based chemotherapy on the brain structural networks are still unclear. Structural magnetic resonance imaging (sMRI) data were collected from 32 NSCLC patients following platinum-based chemotherapy, 36 NSCLC patients without chemotherapy, and 39 healthy controls. Clinical physiological indicators of NSCLC patients were collected. Then, morphological similarity networks were constructed using individual MRI data, and topological properties were calculated using the graph theory method. Differences between the three groups were investigated using one-way ANOVA and two-sample t-test, and relations between the topological properties and clinical physiological indicators were calculated. We found that degree ($F(2,104) = 18.367$, $p < 0.001$) and nodal efficiency ($F(2,104) = 12.546$, $p < 0.001$) in temporal-parietal networks were significantly reduced in NSCLC patients following platinum-based chemotherapy compared to healthy controls/patients without chemotherapy. These changes ($p < 0.05$) were positively correlated with clinical measures, including thrombocytes, granulocytes and hemoglobin, and were negatively correlated with measures of triglycerides and cholesterol levels. Network properties including clustering coefficient ($F(2,104) = 41.435$, $p < 0.001$), number of K-edges ($F(2,104) = 40.304$, $p < 0.001$), density of K-edges ($F(2,104) = 40.304$, $p < 0.001$), global efficiency ($F(2,104) = 42.585$, $p < 0.001$) and small-world ($F(2,104) = 37.132$, $p < 0.001$) were also significantly reduced. These results indicate that platinum-based chemotherapy might cause cerebrovascular damage and clinical indicators’ changes, which then cause the properties of morphological similarity networks’ changes in the temporal and parietal lobes. This study may help us better understand the “chemobrain” in NSCLC patients.

Introduction

Lung cancer ranks first in the global cancer morbidity and mortality ranking, accounting for 11.6% and 18.4% of all incidences of cancer in the population, respectively. Lung cancer can be divided into small cell lung cancer (SCLC) and non-small cell lung cancer (NSCLC), while NSCLC accounts for more than 85% of the total lung cancer cases (Bray et al. 2018). Chemotherapy, radiotherapy, surgery and targeted therapy are commonly used in the clinical treatment of lung cancer patients (Bray et al. 2018). In recent years, a number of neuropsychological studies have shown that lung cancer and chemotherapy have certain negative influences on the executive function and cognitive memory function of patients’ brains (Grosshans et al. 2008; Simo et al. 2013; Simo et al. 2018; Simo et al. 2015; Simo et al. 2016). In previous studies, short transient cognitive impairment in patients with NSCLC after chemotherapy was found (Kaasa, Mastekaasa, and Naess 1988; Simo et al. 2016), and nearly 60–90% of patients with SCLC had cognitive impairment after chemotherapy for 1 to 5 months. Neuroimaging studies have also demonstrated chemotherapy-related brain structural and functional changes in lung cancer patients (Simo et al. 2013; Simo et al. 2018; Simo et al. 2015; Simo et al. 2016). However, whether NSCLC and chemotherapy have a broad effect on brain networks in patients with NSCLC remains unclear.

Previous studies have shown that lung cancer tumors themselves can lead patients to develop paraneoplastic neurological syndrome (PNS) (Graus and Dalmau 2012; Honnorat and Antoine 2007; Leypoldt and Wandinger 2014; Voltz 2002), and cognitive impairment known as “chemobrain” could also be caused by chemotherapy in cancer patients (Ahles and Saykin 2007; Simo et al. 2013; Zeng et al. 2020). First, PNS causes the nervous system distancing effect, which causes symptoms of damage in some parts of the central nervous system, leading to cognitive dysfunction in patients (Leypoldt and Wandinger 2014). The mechanism may be that malignant tumor cells change inflammatory mediators, such as cytokines, chemokines, platelets and neutrophils, in the body environment through the inflammatory response of the tumor microenvironment during the growth process and promote the metabolites of tumor cells to cross the blood–brain barrier and affect the brain (Graus and Dalmau 2012; Leypoldt and Wandinger 2014). Second, drug molecules across the blood–brain barrier react to neurotoxicity in the brain during the process of chemotherapy, and neurons with oxidative damage, cell factor disorders and nerve repair and/or plasticity-related genes of individual variation and other factors may lead to a brain structure in patients with a wide range of morphological changes, functional brain damage, and cognitive impairment (Ahles and Saykin 2007; Hosseini., Koovakkattu., and Kesler. 2012; Janelsins et al. 2011; Wefel, Witgert, and Meyers 2008). In addition, chemotherapeutic drug molecules may induce ischemic lesions, hinder the formation of cerebrovascular blood and reduce cerebrovascular blood flow, thus causing local lesion and functional damage to the cerebral cortex of patients (Simo et al. 2013). Third, recent neuroimaging studies have also found changes in the brain structure networks of lung cancer patients. For example, Liu et al. used diffusion-tensor imaging (DTI) of structural connectivity to analyze the connection network using the graph theory method and found that the topological characteristics of the structural network in the brain of patients with NSCLC before chemotherapy were impaired, the clustering coefficient of the left hippocampus was significantly reduced, and cognitive function was reduced (Liu et al. 2020). Using magnetic resonance imaging (MRI), Simo et al. found that lung cancer patients had speech memory deficits and extensive white matter damage before chemotherapy, while reduced gray matter density and impaired white matter integrity showed impaired visuospatial and verbal fluency after chemotherapy (Simo et al. 2015). Using functional magnetic resonance imaging (fMRI), Simo et al. also found that cognitive deficits induced by lung cancer and chemotherapy resulted in abnormal functional connections related to the default network, left and right anterior temporal lobe network, and cerebellar network and decreased connectivity (Simo et al. 2018). In brief, lung cancer patients’ specific brain networks, which are involved in various functions, such as executive function and cognitive memory, seem to be most vulnerable.

To date, most studies have focused on exploring the changes in lung cancer patients’ brain networks through DTI and fMRI connections (Bromis et al. 2017; Liu et al. 2020), while few methods have been used to construct networks based on the morphological similarities of the gray matter cortex. Cortical morphological data contain a large amount of brain structural connectivity information, while brain structure and brain function interact with each other, and the functional state of the brain may come from the basis of similar brain region structure and morphology (Rubinov and Sporns 2010). The morphological similarity network is based on the structural similarity between each pair of nodes. The

nodes represent the cerebral cortex area and are considered to be connected when they are on the cortical thickness or volume covariant, or when they are shown in a single subject's structural similarity(Tijms et al. 2012; Tijms et al. 2013). Morphological similarity may be a measure of the degree of synchronous development and maturity of brain regions in subjects, reflecting the synergistic change pattern of brain regions' structures; the more similar the structures are, the stronger the connectivity of brain regions is (Alexander-Bloch, Giedd, and Bullmore 2013; He et al. 2009). At present, most studies define the nodes in the brain structural network by the brain regions divided by prior templates, but the brain regions as nodes cannot include more detailed morphological features. Furthermore, the structural network is calculated based on the population level, so the results of networks are at the group level, while the structural network changes for a single individual cannot be measured (Liu et al. 2020; Simo et al. 2018; Simo et al. 2015). Therefore, in our work, individual morphological similarity networks of lung cancer patients were constructed to explore the effects of chemotherapy on patients.

In this study, we first hypothesized that there may be chemotherapy-induced brain structural network changes in patients with NSCLC receiving chemotherapy. The morphological similarity networks (Tijms et al. 2012) of the gray matter were constructed from the NSCLC patients receiving/not receiving chemotherapy and healthy control groups. Then, graph-theoretical properties based on the morphological similarity networks were calculated and compared among the above 3 groups. In addition, relations between those network characteristics and clinical parameters, including granulocytes and thrombocytes, were also investigated.

Materials And Methods

Participants and datasets

A total of 68 patients with non-nervous system metastatic NSCLC [including 36 NSCLC patients without chemotherapy (C-) and 32 NSCLC patients receiving chemotherapy (C+)] and 39 sex-, age- and education-matched healthy controls (HCs) were recruited from Sichuan Cancer Hospital for the current study (Table 1). Patient blood (granulocytes, lymphocytes, hemoglobin, thrombocytes, cholesterol, triglycerides) and tumor (anticarcinogenic embryonic antigen, enolase) indicators were also collected to assess patients' basic metabolism of the immune, digestive and endocrine systems. All patients were diagnosed by the clinician based on clinical information consistent with NSCL-2 (National Comprehensive Cancer Network's clinical practice guidelines in oncology, https://www.nccn.org/guidelines/category_1). The exclusion criteria for participants were as follows: (1) any treatment with psychotropic medication, (2) previous history of severe psychiatric disorders, (3) history of hypertension and diabetes, (4) previous history of any metastatic tumor, (5) any history of neurological disorders, head trauma, stroke or other central nervous system injury or disease, and (6) substance abuse history. Our study was approved by the ethical commission of Sichuan Cancer Hospital and written informed consent was obtained from all participants.

Table 1
Demographic information about the study population.

Variables	HC (n = 39)	Without chemotherapy (n = 36)	Chemotherapy (n = 32)	p-value
Age (years)	48.9 ± 11.9	56.1 ± 8.1	59.1 ± 8.3	0.561†
Sex (male/female)	20/19	24/12	22/10	0.242*
Smoke	6ª (16%)	15 (42%)	17 (53%)	0.003*
Drink	7ª (18%)	6ª (17%)	15 (46%)	0.006*
Chemotherapy drug type	N/A	N/A	Cisplatin (75%) CBP (84.5%) Taxol (34.4%)	N/A

HC: healthy control; N/A: not applicable; CBP: carboplatin; †p-value obtained by ANOVA model. *p-value obtained by two-tailed Pearson chi-square test. These are significant differences between groups ª and .

RI data acquisition

T1-weighted images of all the participants were acquired on a 3.0 T MRI scanner (SIEMENS-AVANTO, Germany). The scanning parameters were as follows: 192 sagittal slices, repetition time (TR) = 1160 ms, echo time (TE) = 4.24 ms, inversion time (TI) = 600 ms, field of view (FOV) = 256×256 mm2, fl, p angle (FA) = 15°, data matrix = 256×256, and voxel size = 1.0×1.0×1.0 mm3.

Brain segmentation

A total of 107 structural brain volumes were segmented into gray matter (GM), white matter (WM), and cerebrospinal fluid (CSF) using the hidden Markov random field (HMRF) model available in CAT12 software (CAT12 release, www.dbm.neuro.uni-jena.de/CAT12/). To normalize the morphological similarity networks of subjects, masks of gray matter images (voxels greater than the mean value of all nonzero voxels) were first generated to obtain denoised gray matter images. Since the network properties may change with the network's size, an intersecting mask was then generated to retain the gray matter image. Therefore, each subject network had the same number of gray matter voxel points, which ensured no difference in the size of networks for each subject.

Morphological similarity networks

Individual morphological similarity networks were extracted from gray matter images using the method proposed by Tijms et al.(Tijms et al. 2012; Tijms et al. 2013). Figure 1 shows the flowchart of analysis. First, the GM segmentation of an individual brain was divided into 3×3×3 mm^3 voxels, which was the minimum spatial resolution that still captures cortical folding that has been shown to be 3 mm (Kiselev,

Hahn, and Auer 2003), and a cube size of 3×3×3 voxels corresponding to a cluster size of 9×9×9 mm^3 was used to obtain a total of 2348 cubes. Each cube represents a node v of each individual network, and each edge represents the morphological similarity of gray matter volume between each pair of cubes. The structural morphological similarity between two cubes v_i and v_j was quantified by the correlation coefficient r_{ij} (Batalle et al. 2013; Tijms et al. 2012):

$$r_{ij} = \frac{\Sigma_{k=1}^{n}(v_{ik}-\overline{v_i})(v_{jk}-\overline{v_j})}{\sqrt{\Sigma_{k=1}^{n}(V_{ik}-\overline{v_i})^2}\sqrt{\Sigma_{k=1}^{n}(V_{jk}-\overline{v_j})^2}}. \qquad (1)$$

where *rik* is the *kth* element in n voxels of cube v_i, and $-v_i$ is the average value of all voxels in cube v_i. Given that the gray matter cortex is a curved structure, two similar cubes may be at the same angle, which may reduce their similarity value. Therefore, we rotated the cube v_i by an angle θ with multiples of 45° around the seed cube v_j and reflected on all axes to find the maximum correlation value r_{jm}^{max} with the target cube *vm*:

$$r_{jm}^{max} = arg_{\theta}^{max}\left(\frac{\Sigma_{i=1}^{n}(v_{ji}(\theta)-\overline{v_j})(v_{mi}-\overline{v_m})}{\sqrt{\Sigma_{i=1}^{n}(V_{ji}(\theta)-\overline{v_j})^2}\sqrt{\Sigma_{i=1}^{n}(V_{mi}-\overline{v_m})^2}}\right). \qquad (2)$$

Next, the similarity network matrices were binarized based on the significance of correlations after determining a threshold for each individual graph with a permutation-based method to ensure a chance of spurious correlations < 5% (SD = 0.002) between cubes. Only the positive similarity values survived this threshold.

Network properties

For the brain network under the sparsity threshold of each individual, we calculated nodal and global network properties. Nodal network properties included connectivity degree, intermediate centrality and nodal efficiency (Boccaletti et al. 2006). The connectivity degree evaluates the number of connections between adjacent nodes, and a node with connections to more adjacent nodes indicates that the function of information interaction is stronger (He, Chen, and Evans 2007). Nodal efficiency evaluates the ability of modular information processing of the network, and a high value indicates that the nodal information exchanges faster (Achard and Bullmore 2007).

Global network properties included the number of K-edges, the density of K-edges, minimum and average path length, clustering coefficient, small-world networks and global efficiency. The number of K-edges is the sum of all nodes in the network, and the density of K-edges is the ratio of the sum of all nodes in the networks to all possible edges, which reflects the path efficiency of network information transmission (Batalle et al. 2013). The minimum average path length is the average of all shortest path lengths between network node pairs, which reflects the information transmission rate of the network. The smaller the value is, the faster the transmission will be (Watts and Strogatz 1998). The clustering coefficient is

equal to the ratio of the actual number of connecting edges and the maximum number of connecting edges among the neighbors of the node. The overall clustering coefficient is the average of all node clustering coefficients, reflecting the possibility of establishing relationships among nodes. The small-world network reflects the ability of topological structure separation and integration of the network, which makes the network distinguishable from regular networks and random networks. The larger the value is, the stronger the integration of network information flow is (Humphries, Gurney, and Prescott 2006). Global efficiency reflects the information exchange mode of the overall brain network; the higher the value is, the larger the information exchange of the brain network is and the more active the neuron cell's activity is (Latora and Marchiori 2001).

Statistical analysis

In the present study, one-way analysis of variance (ANOVA) for age comparison and the chi-square test for sex, smoking, and alcohol consumption comparison were used between NSCLC patients and the HC group. One-way ANOVA was also used to determine the significant differences ($p < 0.001$) among network characteristics of the C+, C- and HC groups, and then a two sample t-test was performed to obtain the significant differences ($p < 0.001$) between pairs of two groups. Finally, relations between clinical measures (e.g., routine blood, biochemical and tumor marker indices) and network properties in altered regions were investigated using partial correlation analysis. Variables including age, sex, smoking, alcohol consumption and cortical total volume were added as covariates in all statistical analyses.

Results

Patient characteristics

No significant differences in age ($F(2,104) = 3.357$, $p = 0.561$) or sex ($\chi^2(2) = 2.840$, $p = 0.242$) were found among the three groups. There were significant differences in smoking ($\chi^2(2) = 11.829$, $p = 0.003$) and drinking ($\chi^2(2) = 10.148$, $p = 0.006$) between the NSCLC patients and the HC group, but there were no significant differences in the patients. Carboplatin and cisplatin combined with other drugs were used in 32 NSCLC patients receiving chemotherapy. The proportion of the number of patients receiving chemotherapy is shown in Table 1, and details of the drug regimen for each patient are shown in supplementary materials Table S2.

Group differences in nodal network measures

Compared with the HC and C- groups, the degrees of the C + group were decreased ($F(2,104) = 18.367$, $p < 0.001$, cluster size = 100, Fig. 2) mainly in the temporal lobe (right inferior temporal gyrus, ITG; bilateral middle temporal gyrus, MTG; right superior temporal gyrus, STG; right temporal pole middle temporal gyrus, TPOmid), right parietal lobe (supramarginal gyrus, SMG; supramarginal and angular gyri of the inferior parietal lobe, IPL; postcentral gyrus, PoCG), as well as a part of the right frontal lobe (orbital part of middle frontal gyrus, ORBmid; orbital part of the inferior frontal gyrus, ORBinf). Significantly decreased ($F(2,104) = 12.546$, $p < 0.001$, cluster size = 100, Fig. 3) nodal efficiency was located in the right temporal

lobe (superior temporal gyrus, STG), right parietal lobe (superior marginal gyrus, SMG), left temporal lobe (inferior temporal gyrus, ITG; middle temporal gyrus, MTG; superior temporal gyrus, STG), left frontal lobe (orbital inferior frontal gyrus, ORBinf), left angular gyrus (ANG) and left middle occipital gyrus (MOG), and details of anatomical regions are shown in the supplementary materials Table S1.

Group differences in global network measures

The global network properties based on morphological similarity networks were further analyzed. All the gray matter structural networks had a small-world $(C_{net}/C_{rand} >> 1 \text{ and } L_{net}/L_{rand} \approx 1).$ Compared with HC and C- patients, clustering coefficient ($p < 0.001$, $F(2,104)=41.435$), number of K-edges ($p < 0.001$, $F(2,104) = 40.304$), density of K-edges ($p < 0.001$, $F(2,104) = 40.304$), global efficiency ($p < 0.001$, $F(2,104) = 42.585$), and small-world ($p < 0.001$, $F(2,104)=37.132$) were significantly decreased in C+ patients, and minimum and average path ($p < 0.001$, $F(2,104)=37.561$) was significantly increased in C+ patients (Fig. 4). There was no significant difference in global network properties between the C- group and the HC group.

Relationships between network and clinical measures

Partial correlations between the network and clinical measures were calculated. Positive correlations between the number of granulocytes and degrees were found in TPOmid. R ($r = 0.433$, $p = 0.021$), MTG. R ($r = 0.488$, $p = 0.008$), ORBinf. R ($r = 0.411$, $p = 0.03$), ORBmid. R ($r = 0.566$, $p = 0.002$), STG. R ($r = 0.501$, $p = 0.007$), SMG. R ($r = 0.393$, $p = 0.038$), PoCG. L ($r = 0.47$, $p = 0.012$), and negative correlations between cholesterol concentration and degrees were found in TPOmid. R ($r=-0.395$, $p = 0.038$), MTG. R ($r=-0.396$, $p = 0.037$). Negative correlations between triglyceride concentration and degrees were located in the ITG. R ($r=-0.521$, $p = 0.005$) and PoCG. L ($r=-0.385$, $p = 0.043$), and a positive correlation between the number of hemoglobin and degrees was found in the MTG. R ($r = 0.502$, $p = 0.006$) (see Fig. 5A). Figure 5B shows that there were significant positive correlations between nodal efficiencies and the number of thrombocytes (STG. L, $r = 0.372$, $p = 0.017$)/number of hemoglobin (MTG. L, $r = 0.317$, $p = 0.043$), and negative correlations between nodal efficiencies and triglyceride concentration (ORBinf. L, $r=-0.317$, $p = 0.043$; STG. L, $r=-0.311$, $p = 0.048$). In addition, significant partial correlations between clinical measures and AAL template-based morphological similarity networks were also found in the C + groups (see Fig. S3 in the supplementary materials).

Discussion

To our knowledge, this study describes for the first time the use of individual morphological similarity networks extracted from GM using standard T1-weighted MRI acquisitions in NSCLC patients. We demonstrated that chemotherapy would induce an altered network topology in NSCLC patients, and those changed network properties may be associated with changes in clinical physiological indicators in NSCLC patients.

Differences of nodal network measures

In the present study, we found that the connectivity degree and nodal efficiency of local nodes in the right temporal-parietal-frontal and left temporal-parietal areas were significantly reduced in the C + group compared with the C- group ($p < 0.001$) (Fig. 2). Similar results were also found in the AAL-based morphologic similarity network analysis (Fig. S2). The connectivity degree reflects the number of connections between local nodes, and the nodal efficiency reflects the modular information processing efficiency or fault tolerance of the network. It is possible that the reduction in both the connectivity degree and nodal efficiency indicated that the information interaction function between nodes may be weakened (Achard and Bullmore 2007; He, Chen, and Evans 2007; He et al. 2009). In addition, significant relations between the nodal network and clinical measures were found in patients (Fig. 5, Figs. S3 and S4). Cisplatin and carboplatin combined with paclitaxel were used as multi-cycle chemotherapy in our study. On the one hand, cisplatin can significantly inhibit angiogenesis (Kirchmair et al. 2005), and paclitaxel, as an anti-angiogenesis drug, may hinder cerebral vascular formation and reduce cerebral vascular blood flow (Simo et al. 2013). In animal models of cisplatin-induced neuropathy, cerebral nerve blood flow and neurovascular levels were significantly reduced, accompanied by significant endothelial cell apoptosis, leading to severe peripheral neuropathy characterized by focal axonal degeneration (Kirchmair et al. 2005). Stewagen et al. found that cisplatin chemotherapy in testicular cancer survivors showed increased vascular damage and accelerated vascular aging with age (Stelwagen et al. 2020). At the same time, studies have shown that platinum drugs may have a slight toxic effect in blood, such that 2–50% of patients have cisplatin-induced platelet reduction, and 0–50% of patients have cisplatin-induced granulocyte reduction (Mckeage 1995). Thrombocytopenia may inhibit neural stem cells from multiplying and developing into neurons (Leiter et al. 2019). Sas et al. found that some neutrophils promote neuronal survival and retinal ganglion cell axon regeneration, and a reduction in the number of neutrophils may inhibit network regeneration (Sas et al. 2020). Our results might imply that in lung cancer patients, thrombocytes, hemoglobin and granulocyte counts were significantly decreased by chemotherapy drugs to inhibit angiogenesis. The cerebral cortex caused reduced blood flow and thus, loss of the oxygen-carrying capacity of hemoglobin, local cortex neuron cell regeneration, and morphological structural damage in the local area. These impacts may be the reason that the local regional connectivity, connectivity efficiency and strength of the temporal-parietal region were significantly reduced.

On the other hand, abnormal metabolism of blood lipids in patients may aggravate morphological and structural damage in the brain. In our study, the concentrations of cholesterol and triglycerides significantly increased in the C + group. Boulware et al. found that breast cancer patients who received platinum drugs showed persistent hypercholesterolemia and triglyceride metabolism disorder, leading to elevated blood lipid levels after chemotherapy (Boulware, Kent, and Frick 2012). Meanwhile, Yin et al. found that sustained high cholesterol and triglyceride levels may lead to language dysfunction (Yin et al. 2012). In our study, abnormal metabolism of blood lipids in patients after chemotherapy may act on local areas of the temporal-parietal region to significantly reduce its connectivity attributes.

The temporal-parietal network is involved in executive control, language processing, episodic memory encoding and declarative memory processing (Eichenbaum, Yonelinas, and Ranganath 2007; Liu et al. 2020; Smith et al. 2009). Previous studies have also examined the influence of platinum drugs on the

temporal-parietal network of patients (Cole and Schneider 2007; Davidson et al. 2008; Hosseini., Koovakkattu., and Kesler. 2012; Mckeage 1995). McKeage et al. showed that cisplatin may induce irreversible hearing loss in the speech range of cancer patients and speculated that the platinum-induced vasospastic response may lead to impaired blood supply to the corresponding brain regions concentrated in the left temporal lobe and reduced blood flow (Mckeage 1995). Hosseini et al. found that the temporal lobe was less efficient after platinum chemotherapy in breast cancer patients, suggesting that the temporal lobe was more susceptible to chemotherapy drugs (Hosseini., Koovakkattu., and Kesler. 2012). Our results were consistent with these findings, suggesting that platinum chemotherapy may lead to abnormal changes in the attributes of the temporal-parietal network, which may affect related cognitive functions. In addition, we found a reduction in connectivity strength and node efficiency in the orbitofrontal region. We speculated that platinum-based drugs may have an effect on other higher cognitive functions associated with the frontal lobe (Dumais et al. 2018; Li et al. 2015).

Differences in global network measures

In this study, the morphological similarity network of all groups had small-world characteristics relative to the random network. Compared with the normal group and patients without chemotherapy ($p < 0.001$), patients receiving chemotherapy demonstrated decreased clustering coefficient, small-world characteristics, number of K-edges, density of K-edges and global efficiency and increased minimum and average path length of the morphologic similarity network (see Fig. 4). These results suggested that lung cancer patients receiving platinum-based chemotherapy were associated with weaker small-world characteristics and lower clustering coefficients. Global efficiency reflects integrated information processing between remote regions of the brain and is mainly related to long-distance connections (Latora and Marchiori 2001). The reduction in global efficiency indicated that the brain network of chemotherapy patients had impaired information transmission, exchange and processing functions at the local and global levels, and its morphologically similar brain network was more random. Hosseini et al. found that the global clustering coefficient, small-world attributes and global efficiency of the brain network decreased in breast cancer patients receiving platinum chemotherapy, and the shortest path length of the temporal lobe and frontal lobe increased, suggesting that multiple brain regions may be impacted by chemotherapy drugs (Hosseini., Koovakkattu., and Kesler. 2012). Kesler et al., using structural neuroimaging provided at the population level analysis, demonstrated the presence of diffuse atrophy and changes in morphological structural network coordination patterns in the gray matter volume of breast cancer patients after chemotherapy (Kesler, Watson, and Blayney 2015). Our results were consistent with these studies and implied that patients with lung cancer who received drug chemotherapy perhaps induced diffuse atrophy of gray matter, which may account for the changes in the overall brain network topographies.

Limitations

First, in the present study, the network characteristics of lung cancer patients in the non-chemotherapy group and the HC group were not significantly changed. The effects of cancer on the brain were previously reported in mostly breast cancer studies (Hosseini., Koovakkattu., and Kesler. 2012; Boulware,

Kent, and Frick 2012; Feng et al. 2019). However, whether and how lung cancer impacts the cerebral cortex needs to be further explored. Second, as a retrospective data study, our work lacks behavioral data of patients, so it is difficult to assess the abnormal effects of chemotherapy on the cognitive functions of patients in the brain. Further evaluation is required in subsequent studies. Third, clinical indicators were routinely measured in patients and did not include measures of brain-derived neurotrophic factors (BDNF) (Rana et al. 2021), which can reflect neuronal injury. In subsequent studies, the types and content of antibodies in the cerebrospinal fluid of patients will be collected to demonstrate our findings in the present work. Fourth, the sample size is limited. In the next study, more modalities, such as functional MRI and EEG, and more samples will be collected.

Conclusions

In this work, individual morphologically similar brain networks were used to investigate the changes in the structural brain network in patients with NSCLC after chemotherapy. Our results suggested that platinum-based chemotherapy in NSCLC patients might cause cerebrovascular damage and changes in clinical indicators, and then cause changes in the properties of morphological similarity brain networks in the temporal and parietal lobes. This may provide imaging evidence to help us better understand the “chemobrain” in NSCLC patients.

Declarations

Funding

The present study was financially supported by the Ministry of Science and Technology of the People’s Republic China (No. 2017YFC0113904), the National Natural Science Foundation of China (No. 81861128001), the CAMS Innovation Fund for Medical Sciences (2019-I2M-5-039), the Sichuan Science and Technology Program (2018JZ0073, 2017SZ0004) and the Science and Technology Bereau of Chengdu (No. 2021YF0501659SN).

Conflicts of interest

All authors have no conflicts of interest to disclose.

Ethics approval

All procedures were approved by the ethical commission of Sichuan Cancer Hospital, and all participants provided written informed consent.

Consent to participate

Not applicable.

Consent for publication

Not applicable.

Availability of data and material

The datasets used in this study are available on request to the corresponding author.

Code availability

Not applicable.

Author Contributions

Conceived and designed the work: Li Dong and Weidong Wang. Analyzed data: Gong Chen and Chuan Wu. Acquired the data: Chuan Wu, Yuan Liu, Zengyi Fang, Liping Luo and Xin Lai. Wrote the manuscript: Gong Chen. All authors revised the work for important intellectual content. All of the authors have read and approved the manuscript.

References

1. Achard, S., & Bullmore, E. (2007). 'Efficiency and cost of economical brain functional networks'. *PLoS Comput Biol*, 3, e17
2. Ahles, T. A., & Saykin, A. J. (2007). 'Candidate mechanisms for chemotherapy-induced cognitive changes'. *Nat Rev Cancer*, 7, 192–201
3. Alexander-Bloch, A., Giedd, J. N., & Bullmore, E. (2013). 'Imaging structural co-variance between human brain regions'. *Nat Rev Neurosci*, 14, 322–336
4. Batalle, D., Munoz-Moreno, E., Figueras, F., Bargallo, N., Eixarch, E., & Gratacos, E. (2013). 'Normalization of similarity-based individual brain networks from gray matter MRI and its association with neurodevelopment in infants with intrauterine growth restriction', *Neuroimage*, 83: 901 – 11
5. Boccaletti, S., Latora, V., Moreno, Y., Chavez, M., & Hwang, D. (2006). 'Complex networks: Structure and dynamics'. *Physics Reports*, 424, 175–308
6. Boulware, M. I., Kent, B. A., & Frick, K. M. (2012). 'The impact of age-related ovarian hormone loss on cognitive and neural function'. *Curr Top Behav Neurosci*, 10, 165–184

7. Bray, F., Ferlay, J., Soerjomataram, I., Siegel, R. L., Torre, L. A., & Jemal, A. (2018). 'Global cancer statistics 2018: GLOBOCAN estimates of incidence and mortality worldwide for 36 cancers in 185 countries'. *CA Cancer J Clin*, 68, 394–424
8. Bromis, K., Kakkos, I., Gkiatis, K., Karanasiou, I. S., & Matsopoulos, G. K. (2017). 'Brain Functional Connectivity in Small Cell Lung Cancer Population after Chemotherapy Treatment: an ICA fMRI Study', *Journal of Physics: Conference Series*, 931
9. Cole, M. W., & Schneider, W. (2007). 'The cognitive control network: Integrated cortical regions with dissociable functions', *Neuroimage*, 37: 343 – 60
10. Davidson, P. S., Anaki, D., Ciaramelli, E., Cohn, M., Kim, A. S., Murphy, K. J. … Levine, B. (2008). 'Does lateral parietal cortex support episodic memory? Evidence from focal lesion patients'. *Neuropsychologia*, 46, 1743–1755
11. Dumais, K. M., Chernyak, S., Nickerson, L. D., & Janes, A. C. (2018). 'Sex differences in default mode and dorsal attention network engagement'. *PLoS One*, 13, e0199049
12. Eichenbaum, H., Yonelinas, A. P., & Ranganath, C. (2007). 'The Medial Temporal Lobe and Recognition Memory'. *Annual Review of Neuroscience*, 30, 123
13. Feng, Y., Zhang, X. D., Zheng, G., & Zhang, L. J. (2019). 'Chemotherapy-induced brain changes in breast cancer survivors: evaluation with multimodality magnetic resonance imaging'. *Brain Imaging Behav*, 13, 1799–1814
14. Graus, F., & Dalmau, J. (2012). 'Paraneoplastic neurological syndromes'. *Curr Opin Neurol*, 25, 795–801
15. Grosshans, D. R., Meyers, C. A., Allen, P. K., Davenport, S. D., & Komaki, R. (2008). 'Neurocognitive function in patients with small cell lung cancer: effect of prophylactic cranial irradiation', *Cancer*, 112: 589 – 95
16. He, Y., Chen, Z., Gong, G., & Evans, A. (2009). 'Neuronal networks in Alzheimer's disease', *Neuroscientist*, 15: 333 – 50
17. He, Y., Chen, Z. J., & Evans, A. C. (2007). 'Small-world anatomical networks in the human brain revealed by cortical thickness from MRI'. *Cereb Cortex*, 17, 2407–2419
18. Honnorat, J., & Antoine, J. C. (2007). 'Paraneoplastic neurological syndromes'. *Orphanet J Rare Dis*, 2, 22
19. Hosseini., S. M., Hadi, D. K., & Shelli, R. K. (2012). 'Altered small-world properties of gray matter networkd in breast cancer',BMC Neurology
20. Humphries, M. D., Gurney, K., & Prescott, T. J. (2006). 'The brainstem reticular formation is a small-world, not scale-free, network'. *Proc Biol Sci*, 273, 503–511
21. Janelsins, M. C., Kohli, S., Mohile, S. G., Usuki, K., Ahles, T. A., & Morrow, G. R. (2011). 'An update on cancer- and chemotherapy-related cognitive dysfunction: current status'. *Semin Oncol*, 38, 431–438
22. Kaasa, S., Mastekaasa, A., & Naess, S. (1988). 'Quality of life of lung cancer patients in a randomized clinical trial evaluated by a psychosocial well-being questionnaire'. *Acta Oncol*, 27, 335–342

23. Kesler, S. R., Watson, C. L., & Blayney, D. W. (2015). 'Brain network alterations and vulnerability to simulated neurodegeneration in breast cancer'. *Neurobiol Aging*, 36, 2429–2442
24. Kirchmair, R., Walter, D. H., Ii, M., Rittig, K., Tietz, A. B., Murayama, T. … Losordo, D. W. (2005). 'Antiangiogenesis mediates cisplatin-induced peripheral neuropathy: attenuation or reversal by local vascular endothelial growth factor gene therapy without augmenting tumor growth'. *Circulation*, 111, 2662–2670
25. Kiselev, V. G., Klaus, R., Hahn, & Auer, D. P. (2003). 'Is the brain cortex a fractal?'. *Neuroimage*, 20, 1765–1774
26. Latora, V., & Marchiori, M. (2001). 'Efficient behavior of small-world networks'. *Phys Rev Lett*, 87, 198701
27. Leiter, O., Seidemann, S., Overall, R. W., Ramasz, B., Rund, N., Schallenberg, S. … Kempermann, G., and T. L. Walker. 2019. 'Exercise-Induced Activated Platelets Increase Adult Hippocampal Precursor Proliferation and Promote Neuronal Differentiation',Stem Cell Reports, 12:667–79
28. Leypoldt, F., & Wandinger, K. P. (2014). 'Paraneoplastic neurological syndromes'. *Clin Exp Immunol*, 175, 336–348
29. Li, H. J., Hou, X. H., Liu, H. H., Yue, C. L., Lu, G. M., & Zuo, X. N. (2015). 'Putting age-related task activation into large-scale brain networks: A meta-analysis of 114 fMRI studies on healthy aging'. *Neurosci Biobehav Rev*, 57, 156–174
30. Liu, S., Li, X., Ma, R., Cao, H., Jing, C., Wang, Z. … Wu, J. (2020). 'Cancer-associated changes of emotional brain network in non-nervous system metastatic non-small cell lung cancer patients: a structural connectomic diffusion tensor imaging study'. *Transl Lung Cancer Res*, 9, 1101–1111
31. Mckeage, M. J. (1995). 'Comparative Adverse Effect Profiles of Platinum Drugs'. *Drug Saf*, 13, 228–244
32. Rana, T., Behl, T., Sehgal, A., Srivastava, P., & Bungau, S. (2021). 'Unfolding the Role of BDNF as a Biomarker for Treatment of Depression'. *J Mol Neurosci*, 71, 2008–2021
33. Rubinov, M., & Sporns, O. (2010). 'Complex network measures of brain connectivity: uses and interpretations'. *Neuroimage*, 52, 1059–1069
34. Sas, A. R., Carbajal, K. S., Jerome, A. D., Menon, R., Yoon, C., Kalinski, A. L. … Segal, B. M. (2020). 'A new neutrophil subset promotes CNS neuron survival and axon regeneration'. *Nat Immunol*, 21, 1496–1505
35. Simo, M., Rifa-Ros, X., Rodriguez-Fornells, A., & Bruna, J. (2013). 'Chemobrain: a systematic review of structural and functional neuroimaging studies'. *Neurosci Biobehav Rev*, 37, 1311–1321
36. Simo, M., Rifa-Ros, X., Vaquero, L., Ripolles, P., Cayuela, N., Jove, J. … Rodriguez-Fornells, A. (2018). 'Brain functional connectivity in lung cancer population: an exploratory study'. *Brain Imaging Behav*, 12, 369–382
37. Simo, M., Root, J. C., Vaquero, L., Ripolles, P., Jove, J., Ahles, T. … Rodriguez-Fornells, A. (2015). 'Cognitive and brain structural changes in a lung cancer population'. *J Thorac Oncol*, 10, 38–45

38. Simo, M., Vaquero, L., Ripolles, P., Gurtubay-Antolin, A., Jove, J., Navarro, A. … Rodriguez-Fornells, A. (2016). 'Longitudinal Brain Changes Associated with Prophylactic Cranial Irradiation in Lung Cancer'. *J Thorac Oncol*, 11, 475–486
39. Smith, S. M., Peter, T., Fox, K. L., Miller, D. C., Glahn, P., Mickle Fox, C. E. … Laird (2009). and Christian F. Beckmann. 'Correspondence of the brain's functional architecture during activation and rest', *Proceedings of the National Academy of Sciences of the United States of America*: 13040-45
40. Stelwagen, J., Lubberts, S., Steggink, L. C., Steursma, G., Kruyt, L. M., Donkerbroek, J. W. … Gietema, J. A. (2020). 'Vascular aging in long-term survivors of testicular cancer more than 20 years after treatment with cisplatin-based chemotherapy'. *Br J Cancer*, 123, 1599–1607
41. Tijms, B. M., Moller, C., Vrenken, H., Wink, A. M., de Haan, W., van der Flier, W. M. … Barkhof, F. (2013). 'Single-subject grey matter graphs in Alzheimer's disease'. *PLoS One*, 8, e58921
42. Tijms, B. M., Series, P., Willshaw, D. J., & Lawrie, S. M. (2012). 'Similarity-based extraction of individual networks from gray matter MRI scans'. *Cereb Cortex*, 22, 1530–1541
43. Voltz, R. (2002). 'Paraneoplastic neurological syndromes: an update on diagnosis, pathogenesis, and therapy'. *The Lancet Neurology*, 1, 294–305
44. Watts, D. J., & Strogatz, S. H. (1998). 'Collective dynamics of ‘small-world’ networks'. *Nature*, 393, 440–442
45. Wefel, J. S., Witgert, M. E., & Meyers, C. A. (2008). 'Neuropsychological sequelae of non-central nervous system cancer and cancer therapy'. *Neuropsychol Rev*, 18, 121–131
46. Yin, Z. X., Shi, X. M., Kraus, V. B., Fitzgerald, S. M., Qian, H. Z., Xu, J. W. … Zeng, Y. (2012). 'High normal plasma triglycerides are associated with preserved cognitive function in Chinese oldest-old'. *Age Ageing*, 41, 600–606
47. Zeng, Y., Dong, J., Huang, M., Zhang, J. E., Zhang, X., Xie, M., & Wefel, J. S. (2020). 'Nonpharmacological interventions for cancer-related cognitive impairment in adult cancer patients: A network meta-analysis'. *Int J Nurs Stud*, 104, 103514

Figures

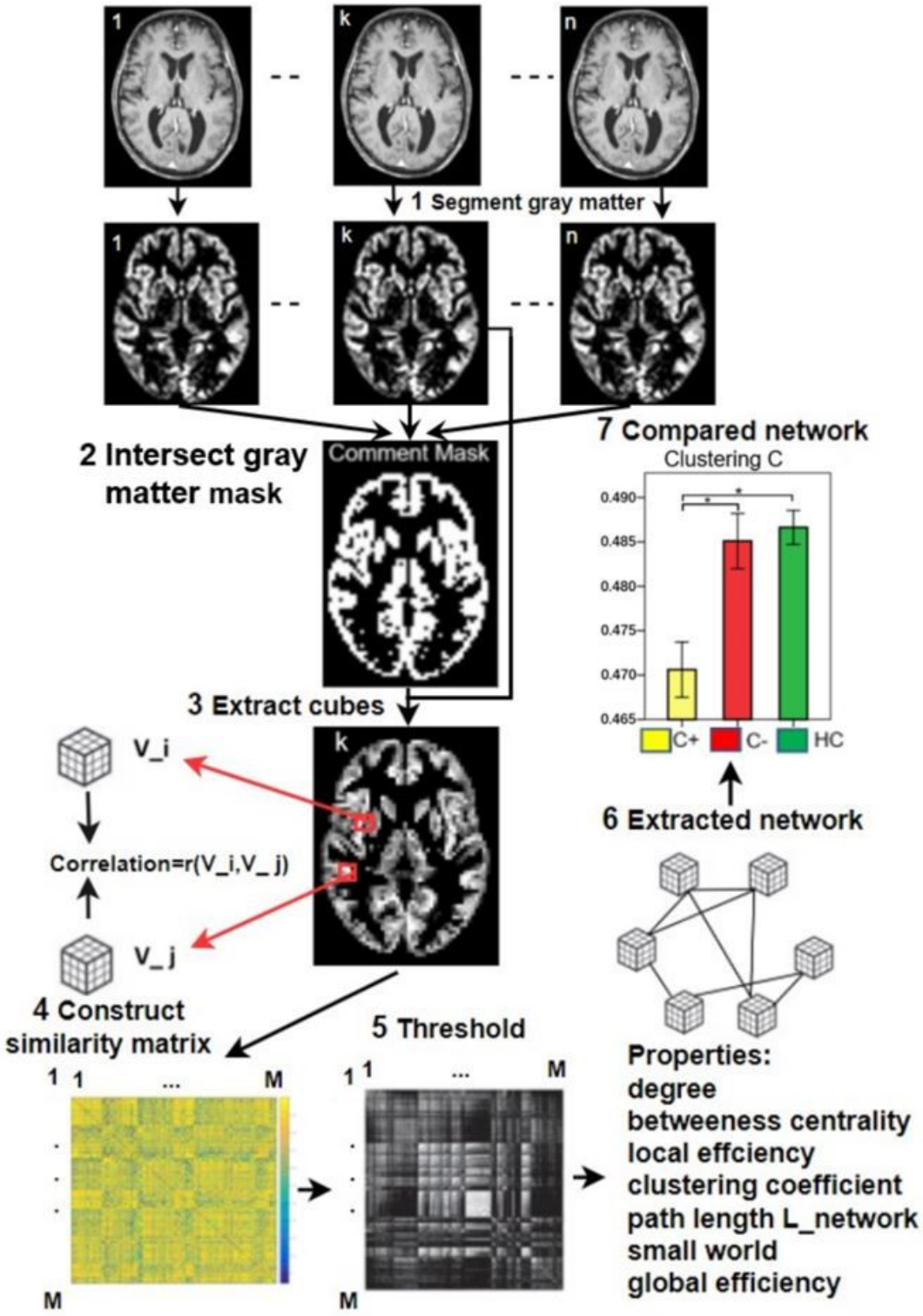

Figure 1

The flowchart of constructing individual morphological similarity networks. (1) Each brain volume was segmented into GM, WM, and CSF. (2) An intersecting gray mask of all 107 subjects was then generated to retain the gray matter image. (3) The gray matter was divided into 3×3×3 voxel cubes. The red arrows point to 2 example cubes and . (4) The similarities among all cubes (M=2348) were computed using the maximum correlation coefficient, storing the result in a matrix with 1 to M rows and columns. (5)

Similarity matrices were binarized, with a threshold that ensured a 5% chance of spurious connections for all individuals (corresponding to a significance level of $p < 0.05$ corrected for multiple comparisons by an FDR technique using an empirical null distribution). (6) The topological properties of the networks were calculated. (7) The topological properties of the networks were compared.

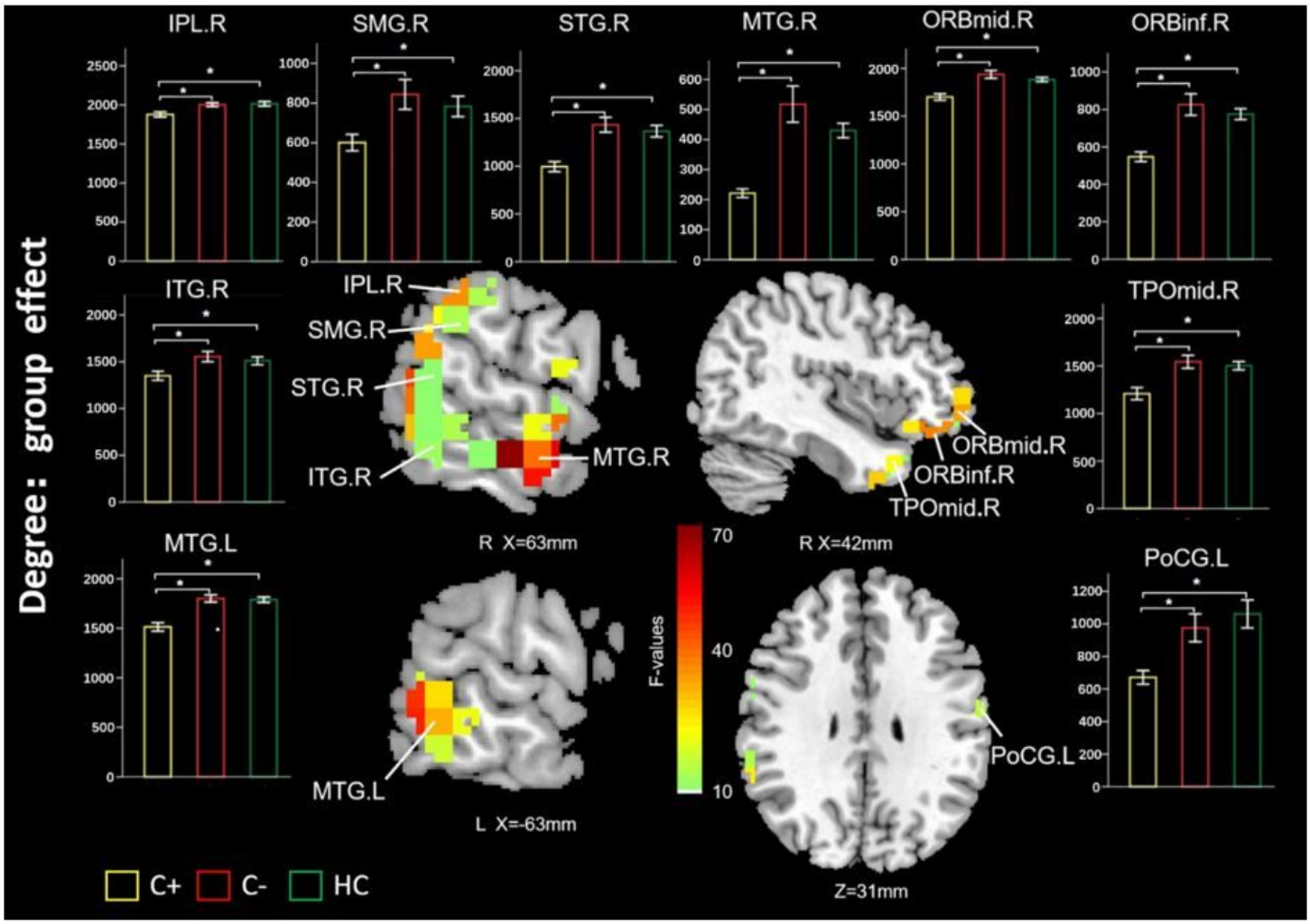

Figure 2

Significant differences between the degrees of C+, C- and HC groups. The significance of F-test is set as $p<0.001$, uncorrected, $F(2,104)=18.367$, cluster size=100; * represents significance of two sample t-test $p<0.001$; C+: NSCLC patients receiving chemotherapy; C-: NSCLC patients without chemotherapy; HC, healthy controls.

Figure 3

Significant differences between the nodal efficiency of the C+, C- and HC groups. The significance of F-test is set as $p<0.001$, uncorrected, $F(2,104)=12.546$, cluster size=100; * represents significance of two

sample t-test p<0.001; C+: NSCLC patients receiving chemotherapy; C-: NSCLC patients without chemotherapy; HC, healthy controls.

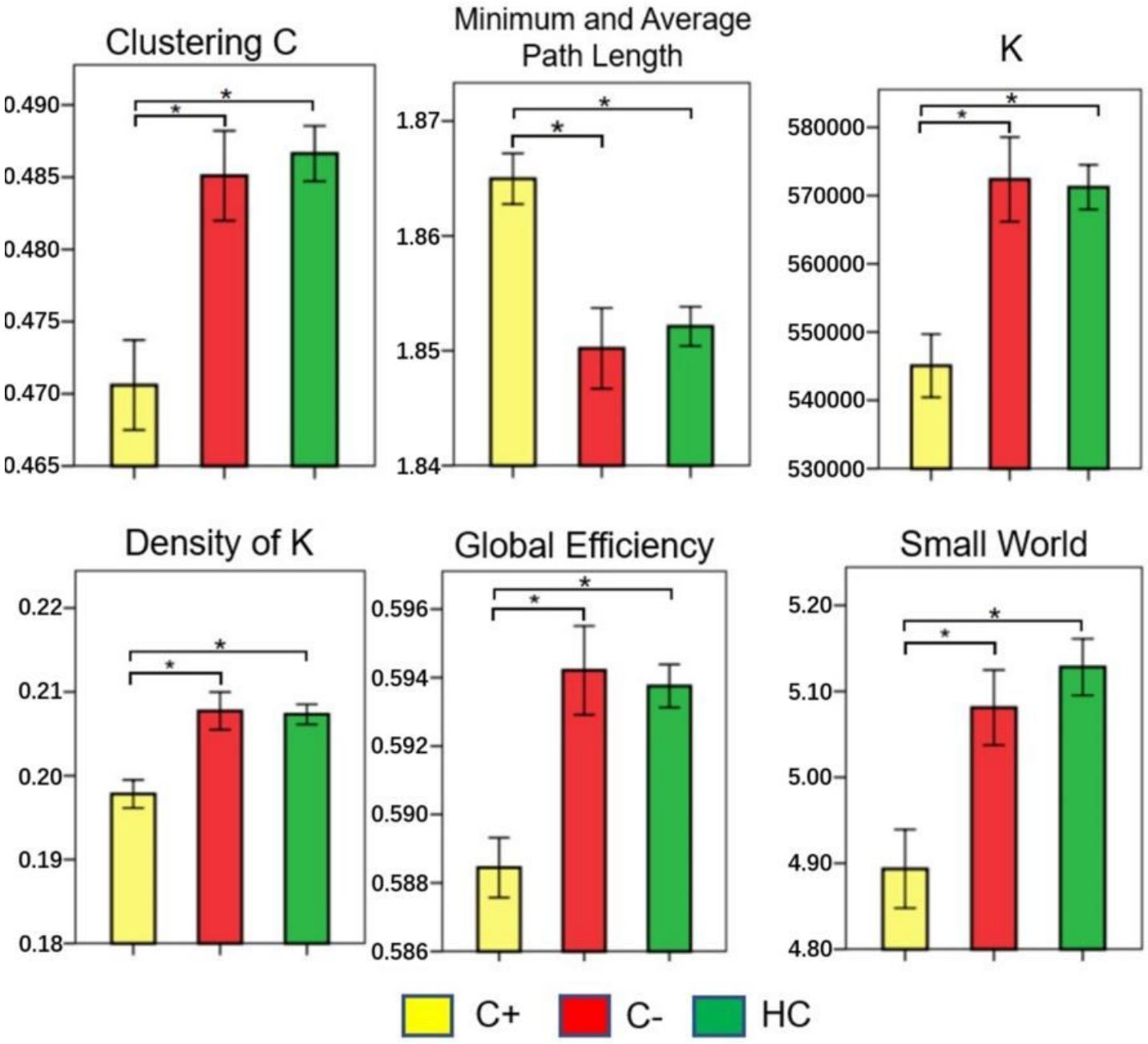

Figure 4

Significant differences in clustering coefficient (Clustering C), minimum and average path length, number of K-edges (K), density of K-edges (density of K), global efficiency and small-world among the 3 groups. NSCLC, non-small-cell lung cancer; C+: NSCLC patients receiving chemotherapy; C-: NSCLC patients without chemotherapy; HC, healthy controls. * represents p<0.001.

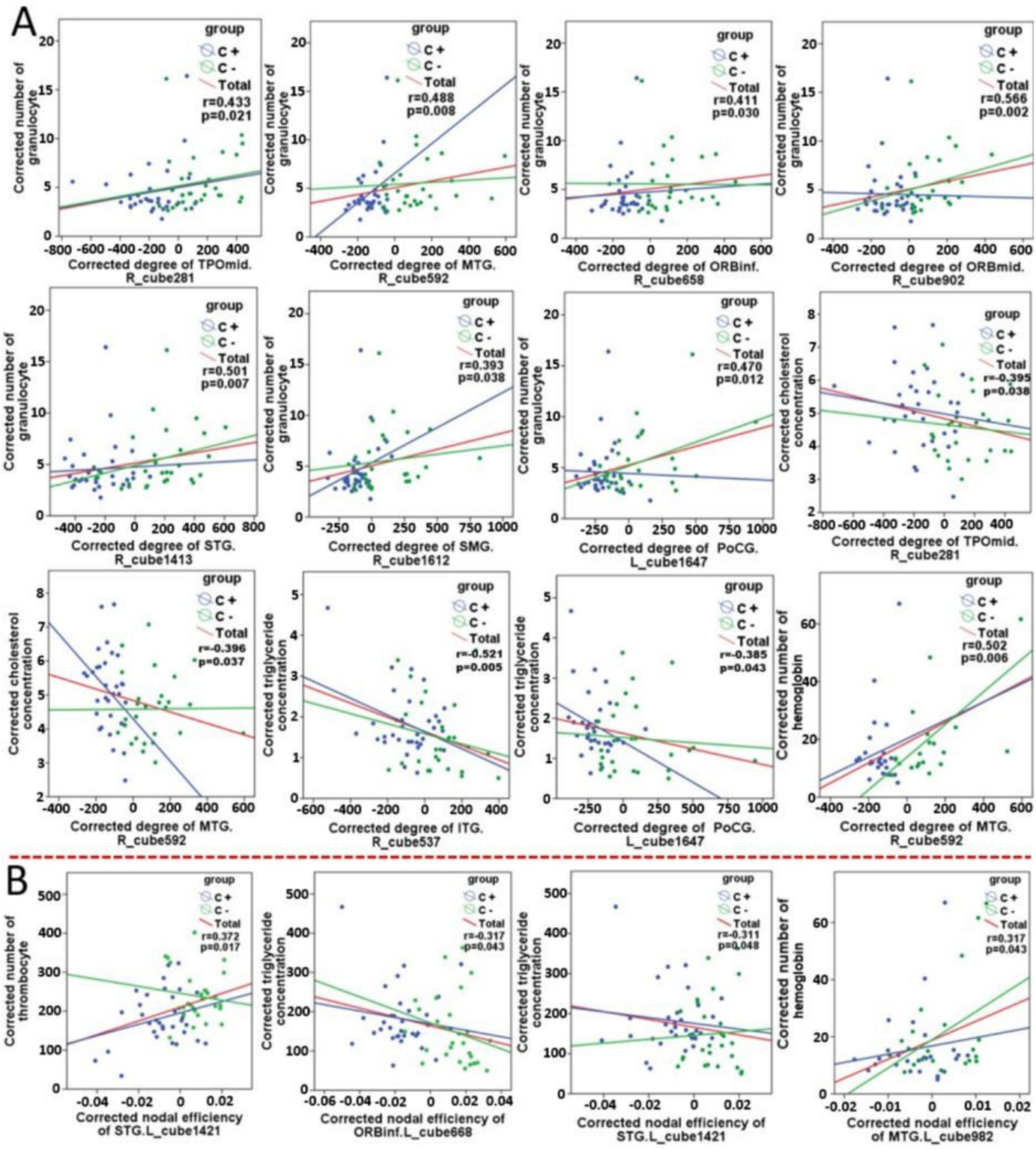

Figure 5

(A) Partial correlations between clinical measures and degrees in the patient group; (B) Partial correlations between clinical measures and nodal efficiency in the patient group. Red line: all patients; blue line: C+ group; green line: C- group.

Supplementary Files

This is a list of supplementary files associated with this preprint. Click to download.

- AuthorChecklist.pdf
- supplementarymaterials.docx